A method to Start Rotating Induction Motor Based on Speed Sensorless Model Predictive Control

Haitao Yang, *Student Member, IEEE,* Yongchang Zhang, *Member, IEEE,* Paul Walker, Nong Zhang and Bo Xia

***Abstract*—In some cases, such as restarting after power interruption and starting a motor rotated by external load, the motor is rotating before being powered by the inverter. For speed-sensorless operation, as both the initial rotational direction and speed is unknown, it would be problematic to achieve smooth and fast resumption of normal operation if the starting scheme is not deliberately designed. In this paper, a method based on adaptive full order observer (AFO) is proposed to address this problem. For AFO without properly designed feedback gain matrix, the estimated speed can not converge to the actual speed if initial estimated speed is significantly lower than the actual speed. Through analyzing transfer function of stator current error, the convergence condition of speed estimation is deduced. A feedback gain matrix and the condition for shifting to normal operation are subsequently proposed to improve the performance. The detailed design and implementation of the proposed method combined with finite control set model predictive flux control (FCS-MPFC) is illustrated. Simulation and experimental results validate the effectiveness of the developed schemes.**

***Index Terms*—Full order observer, model predictive control, restarting, speed sensorless**

NOMENCLATURE

Symbols

$\boldsymbol{i}$	Current Vector
$\boldsymbol{u}$	Voltage Vector
$\boldsymbol{\psi}$	Flux Vector
L, R	Inductance and resistance
ω	Angular frequency
T	Time
j	Imaginary component of a complex variable
s	Laplace operator
g, k	Gain
$\triangle$	Difference
e	Error
θ	Angle
p	Differential operator

Subscripts

s, m, r	Stator, mutual, and rotor

Superscripts

ref	Reference value
$\hat{}$	Estimated value

I. INTRODUCTION

Finite control set-model predictive control (FCS-MPC) is emerging as an effective control method for power converters and motor drives [1]–[5]. It is simple for handling various control objectives and constrains, presenting good dynamic behavior and ability to operate at optimized points. It is shown in [6], [7] that steady state performance of FCS-MPC can be comparable to that of conventional linear controller, while the dynamic performance is much better. Though there is a good prospect of MPC, some aspects such as parameter robustness [1], weighting factor design [8] and sensorless operation [9] should be further investigated to improve its practicability.

During the past decade, much research has been performed to improve the performance of FCS-MPC for application to motor drives. For high power medium voltage drives, solving the optimization problem with long prediction horizon is a major challenge. Various methods, such as branch and bound [2] and sphere decoding [4] are proposed, showing improved performance when extending the prediction horizon. For low and medium power drives, as the switching loss is not the main concern, much research is carried out to reduce the complexity, improve the performance and extend the application range from different types of motors to different converter topologies. To avoid nontrivial weighting factor tuning effort for torque and flux control, the model predictive flux control (MPFC) is proposed in [5]. In MPFC, two scalar references, torque and flux magnitude references, are equivalently converted into a single reference of stator flux vector. While in [8], the prediction errors of different control variables are converted into ranking values. The voltage vector which leads to minimal average ranking value is selected as the best one. For obtaining better steady state performance, the duty cycle optimization is introduced in [10]. In such method, an active voltage vector and a zero vector are applied in one control period to achieve more precise torque control. In [11], the switching instant of new selected voltage vector is not fixed at the beginning of next control period but optimized for reducing torque ripple.

Speed sensorless operation is preferred in many applications because of lower cost and better environmental adaptability. Various methods, such as model reference system [12], Kalman filter [3], [13] and adaptive full order observer (AFO) [14] have been investigated. These sensorless schemes have also been implemented and tested in FCS-MPC [1], [3], [9], achieving satisfactory performance over a wide speed range. But none of them clearly address the problem of starting a free-running motor. Starting a rotating motor is required in many applications, such as resumption of normal operation after power interruption, cut-in control of wind turbine [15] and re-powering after coasting condition of railway traction [16]. As the initial speed is unknown with speed sensorless operation, a large inrush current may occur due to the difference between

the injected frequency of the inverter and rotating frequency of the motor. Hence, a proper scheme should be designed to achieve a safe and quick start of a rotating motor.

AFO is widely studied because it presents good accuracy and parameter robustness over a wide speed range by introducing the feedback of stator current error. The study of AFO is mainly focused on improving its stability, robustness and accuracy during low speed operation [17]–[20]. There is limited research investigating its performance for starting a rotating motor with unknown initial speed. In most cases, it is assumed that the motor is started from standstill. However, when the motor is rotating at a high speed, the estimated speed with a zero initial value may not converge to the actual speed. In [21], a series of estimation method to detect rotational direction and speed for free-running motors are proposed. However, many of them require a proportional-integral (PI) controller and modulator to regulate the injected stator current, which is generally unavailable in FCS-MPC. Additionally, the methods by detecting current responses with specifically injected voltage are not suitable for normal operation. In [22], when AFO is enabled during restarting procedure, the initial estimated speed is set as rated speed. However, if the motor can rotate at both forward and backward direction, the rotational direction must be first estimated to decide whether positive or negative rated frequency is imposed. This increases the complexity of starting process. As starting a free running motor has not been clearly addressed in much previous research of FCS-MPC, a method will be proposed in this paper to cope with this problem.

The main contribution of this paper is the proposed speed sensorless FCS-MPFC can achieve smooth and quick start of a free-running motor. The proposed method is simple and effective, which is not only suitable for initial speed estimation but also applicable for normal operation. First, the convergence condition of estimated speed based on AFO is deduced. Then, a feedback gain matrix is proposed to ensure a successful start with any initial speed. Finally, its detailed implementation combined with FCS-MPFC [5] is demonstrated with simulation and experimental verification. Throughout this paper, parameter mismatches are not addressed. And, it is assumed that machine parameters are already identified with good accuracy.

II. Basic Equations of IM

When stator flux $\boldsymbol{\psi}_s$ and stator current $\boldsymbol{i}_s$ are selected as state variables in stationary frame, the electrical model of IM can be expressed as:

$$p\boldsymbol{x} = \boldsymbol{A}\boldsymbol{x} + \boldsymbol{B}\boldsymbol{u} \tag{1}$$

$$\boldsymbol{A} = \begin{bmatrix} -\lambda(R_s L_r + R_r L_s) + j\omega_r & \lambda(R_r - jL_r\omega_r) \\ -R_s & 0 \end{bmatrix} \tag{2}$$

$$\boldsymbol{B} = \begin{bmatrix} \lambda L_r \\ 1 \end{bmatrix} \tag{3}$$

where, $\boldsymbol{x} = \begin{bmatrix} \boldsymbol{i}_s & \boldsymbol{\psi}_s \end{bmatrix}^T$ and $\lambda = 1/(L_s L_r - L_m^2)$. The rotor flux $\boldsymbol{\psi}_r$ can be calculated using $\boldsymbol{\psi}_s$ and $\boldsymbol{i}_s$ as

$$\boldsymbol{\psi}_r = \frac{\lambda L_r \boldsymbol{\psi}_s - \boldsymbol{i}_s}{\lambda L_m} \tag{4}$$

The electromagnetic torque can be expressed as

$$T_e = \frac{3}{2} N_p \boldsymbol{\psi}_s \otimes \boldsymbol{i}_s \tag{5}$$

where N_p is the number of pole pairs, $\otimes$ represents cross product.

III. Adaptive Full Order Observer

A. Mathematical Equations of AFO

Based on (1), the AFO can be constructed as follows [23]

$$p\hat{\boldsymbol{x}} = \hat{\boldsymbol{A}}\hat{\boldsymbol{x}} + \boldsymbol{B}\boldsymbol{u}_s + \boldsymbol{G}(\boldsymbol{i}_s - \hat{\boldsymbol{i}}_s) \tag{6}$$

where $\boldsymbol{G}$ is the feedback gain matrix of AFO.

$$\boldsymbol{G} = \begin{bmatrix} \boldsymbol{g}_1 \\ \boldsymbol{g}_2 \end{bmatrix} = \begin{bmatrix} g_{1r} + j \cdot g_{1i} \\ g_{2r} + j \cdot g_{2i} \end{bmatrix} \tag{7}$$

Based on Lyapunov's theorem, the adaptive law of estimated speed can be obtained as [24]:

$$p\hat{\omega}_r = \left(\boldsymbol{i}_s - \hat{\boldsymbol{i}}_s\right) \otimes \left(\lambda L_r \hat{\boldsymbol{\psi}}_s - \hat{\boldsymbol{i}}_s\right) \tag{8}$$

$$= \left|\boldsymbol{i}_s - \hat{\boldsymbol{i}}_s\right| \cdot \left|\lambda L_r \hat{\boldsymbol{\psi}}_s - \hat{\boldsymbol{i}}_s\right| \sin\theta \tag{9}$$

where θ is the difference of phase angle between the vector $\lambda L_r \hat{\boldsymbol{\psi}}_s - \hat{\boldsymbol{i}}_s$ and $\boldsymbol{i}_s - \hat{\boldsymbol{i}}_s$, namely

$$\theta = \text{angle}(\lambda L_r \hat{\boldsymbol{\psi}}_s - \hat{\boldsymbol{i}}_s) - \text{angle}(\boldsymbol{i}_s - \hat{\boldsymbol{i}}_s) \tag{10}$$

B. Analysis of AFO during Starting Process

According to (1) and (6), the dynamic equation of error can be derived as

$$\begin{bmatrix} s\boldsymbol{e}_i \\ s\boldsymbol{e}_\psi \end{bmatrix} = F \begin{bmatrix} \boldsymbol{e}_i \\ \boldsymbol{e}_\psi \end{bmatrix} + H \begin{bmatrix} \hat{\boldsymbol{i}}_s \\ \hat{\boldsymbol{\psi}}_s \end{bmatrix} \tag{11}$$

$$F = \begin{bmatrix} a_1 + j\omega_r - \boldsymbol{g}_1 & \lambda R_r - j\lambda L_r \omega_r \\ -R_s - \boldsymbol{g}_2 & 0 \end{bmatrix} \tag{12}$$

$$H = \begin{bmatrix} j \triangle \omega_r & -j\lambda L_r \triangle \omega_r \\ 0 & 0 \end{bmatrix} \tag{13}$$

$$a_1 = -\lambda(R_s L_r + R_r L_s) \tag{14}$$

where, $\boldsymbol{e}_i = \boldsymbol{i}_s - \hat{\boldsymbol{i}}_s$, $\boldsymbol{e}_\psi = \boldsymbol{\psi}_s - \hat{\boldsymbol{\psi}}_s$, $\triangle\omega_r = \omega_r - \hat{\omega}_r$. Based on (11), the following transfer function can be obtained

$$C(s) = \frac{\boldsymbol{e}_i}{\left(\lambda L_r \hat{\boldsymbol{\psi}}_s - \hat{\boldsymbol{i}}_s\right)} = \frac{-j \triangle \omega_r \cdot s}{s^2 + ms + n} \tag{15}$$

where

$$m = \lambda(R_s L_r + R_r L_s) + g_{1r} - j(\omega_r - g_{1i}) \tag{16}$$

$$n = \lambda R_r(R_s + g_{2r}) + \lambda L_r \omega_r g_{2i} - j \cdot y \tag{17}$$

$$y = \lambda L_r \omega_r (R_s + g_{2r}) - \lambda R_r g_{2i} \tag{18}$$

Since torque reference is set as zero during the estimation of free-running speed (slip frequency is assumed to be zero), the

injected frequency will be $\hat{\omega}_r$. Thus, the following transfer characteristic of (15) can be calculated as

$$C(j\hat{\omega}_r) = \frac{|\boldsymbol{e}_i|}{\left|\lambda L_r \hat{\boldsymbol{\psi}}_s - \hat{\boldsymbol{i}}_s\right| \cdot e^{j\theta}} = \frac{\triangle\omega_r\hat{\omega}_r}{(d_1 + j \cdot d_2)} \tag{19}$$

$$d_1 = \hat{\omega}_r(\triangle\omega_r - g_{1i}) + \lambda R_r(R_s + g_{2r}) + \lambda L_r \omega_r g_{2i} \tag{20}$$

$$d_2 = \hat{\omega}_r\left(\lambda(R_s L_r + R_r L_s) + g_{1r}\right) - y \tag{21}$$

Now, the following Lyapunov function is defined.

$$V = \frac{(\omega_r - \hat{\omega}_r)^2}{2} \tag{22}$$

Supposing that ω_r is constant during one control period [23], the time derivative of V is

$$pV = -(\omega_r - \hat{\omega}_r) \cdot p\hat{\omega}_r \tag{23}$$

$\hat{\omega}_r$ will always approach to ω_r, if

$$pV < 0 \tag{24}$$

Namely, if equation (25) holds, the estimated speed $\hat{\omega}_r$ will converge to the actual speed ω_r.

$$\text{sign}(\omega_r - \hat{\omega}_r) \cdot p\hat{\omega}_r > 0 \tag{25}$$

Based on (15) and (19), $\sin\theta$ in (9) can be calculated as

$$\sin\theta = \frac{\triangle\omega_r\hat{\omega}_r \cdot d_2}{|\triangle\omega_r\hat{\omega}_r|\sqrt{(d_1)^2 + (d_2)^2}} \tag{26}$$

Hence, if (27) holds during the whole restarting process, the value of $\sin\theta$ in (9) will change the sign along with $\triangle\omega_r$, so that (25) will be always satisfied.

$$\text{sign}(\hat{\omega}_r) \cdot d_2 > 0 \tag{27}$$

By solving (27), if feedback gain matrix G is set as zero, the following equations can be obtained

$$\hat{\omega}_r > k \cdot \omega_r, \text{ if } \omega_r > 0 \tag{28}$$

$$\hat{\omega}_r < k \cdot \omega_r, \text{ if } \omega_r < 0 \tag{29}$$

where $k = R_s L_r/(R_s L_r + R_r L_s)$. From above condition, it can be found that if the absolute value of $\hat{\omega}_r$ is much smaller than that of ω_r, $\hat{\omega}_r$ will not converge to the actual speed ω_r. As $k < 1$, the motor can be always started by setting the initial estimated speed as

$$\begin{cases} \hat{\omega}_r & = \omega_{max} \quad \text{if } \omega_r > 0 \\ \hat{\omega}_r & = -\omega_{max} \text{ if } \omega_r < 0 \end{cases} \tag{30}$$

where ω_{max} is the absolute value of maximum rotational speed. This means that the rotational direction must be estimated at the beginning. However, if there is a detection error in rotational direction, the estimated speed will converge to zero. This is because once $\hat{\omega}_r$ cross zero, (25) will not be satisfied.

To avoid the dependence of speed information in (19), $\boldsymbol{g}_2$ can be chosen as

$$\boldsymbol{g}_2 = -R_s \tag{31}$$

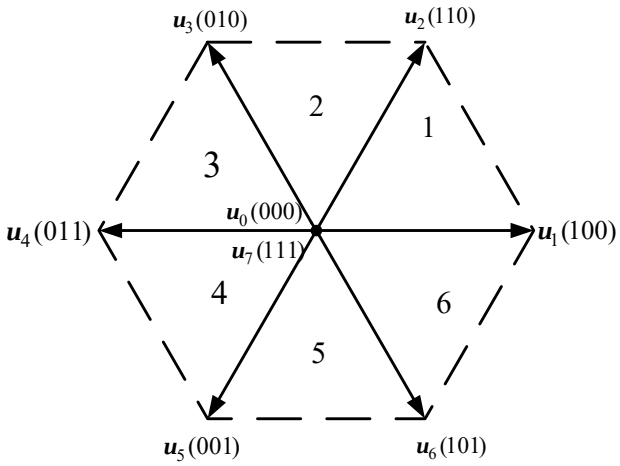

Fig. 1. Switching states and voltage vectors of a two-level inverter

Then, (19) can be rewritten as

$$C(j\hat{\omega}_r) = \frac{\triangle\omega_r}{(\triangle\omega_r - g_{1i}) + j \cdot d} \tag{32}$$

$$d = \lambda(R_s L_r + R_r L_s) + g_{1r} \tag{33}$$

Similar to the deduction of (27), equation (34) should be guaranteed in order to satisfy (25).

$$d > 0 \tag{34}$$

It is seen from (33) that proper initial value of $\hat{\omega}_r$ is no longer required to ensure convergence. g_{1r} can be obtained by solving (34) as

$$g_{1r} = h \cdot \lambda(R_s L_r + R_r L_s) \tag{35}$$

$$h > -1 \tag{36}$$

As g_{1i} has no impact in this study, it is simply set as zero. Hence, the proposed feedback gain matrix can be summarized as

$$\boldsymbol{G} = \begin{bmatrix} h \cdot \lambda(R_s L_r + R_r L_s) \\ -R_s \end{bmatrix} \tag{37}$$

IV. Model Predictive Flux Control

A. Basic principle of MPFC

In [5] , the predictive flux control is introduced to avoid the nontrivial tuning effort for the weighting factor, which is generally required for simultaneously control of flux magnitude and torque in conventional MPTC. The control diagram is shown in 2. The rotor speed is controlled by a proportional-integral (PI) controller.

In MPFC, references of torque T_e^{ref} and flux magnitude ψ^{ref} are equivalently converted as a reference of stator flux vector, as shown in (38) [5] .

$$\begin{cases} \boldsymbol{\psi}_s^{ref} & = \psi^{ref} \exp(j \cdot \angle\boldsymbol{\psi}_s^{ref}) \\ \angle\boldsymbol{\psi}_s^{ref} & = \angle\boldsymbol{\psi}_r + \arcsin\left(\frac{T_e^{ref}}{\frac{3}{2}N_p\lambda L_m|\boldsymbol{\psi}_r|\psi^{ref}}\right) \end{cases} \tag{38}$$

Considering the compensation of one-step delay due to digital implementation, two-step prediction are employed here

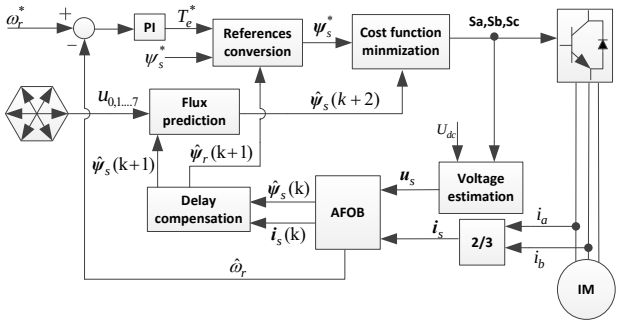

Fig. 2. Control diagram of speed sensorless MPFC

[5], [6], [8]. A cost function can be constructed as (39) to track $\boldsymbol{\psi}_s^{ref}$.

$$J = |\boldsymbol{\psi}_s^{ref} - \boldsymbol{\psi}_s^{k+2}| \tag{39}$$

First, $\boldsymbol{i}_s^{k+1}$ and $\boldsymbol{\psi}_s^{k+1}$ are calculated based on model (1) using the optimal voltage vector selected in the previous control period. Then, the stator flux is predicted using voltage model as

$$\boldsymbol{\psi}_s^{k+2} = \boldsymbol{\psi}_s^{k+1} + T_{sc}(\boldsymbol{u}_s^{k+1} - R_s \boldsymbol{i}_s^{k+1}) \tag{40}$$

For a two level inverter, there are 8 switching states and 7 different voltage vectors, as shown in Fig. 1. After each feasible voltage vector are evaluated by the cost function (39), the best one resulting in a minimal value of (39) is selected as the output for the next control period. More details about MPFC can be found in [5] and are not repeated here. In the next subsection, the original MPFC is slightly modified in conjunction with the proposed AFO to make the controller have the ability to start a rotating motor smoothly and quickly.

During high speed operation, the voltage drop across stator resistance is negligible. If a circular flux trajectory is adopted, the required voltage can be approximated as $\boldsymbol{u}_s = p\boldsymbol{\psi}_s = j\omega_e \boldsymbol{\psi}_s$. In practical application, the trajectory of $\boldsymbol{u}_s$ should be inside of the hexagon as shown in Fig. 1. Hence, the maximum magnitude of stator flux should satisfy the following equation.

$$\omega_e \, |\boldsymbol{\psi}_s| < \frac{U_{dc}}{\sqrt{3}} \tag{41}$$

Considering constraint of (41), the flux magnitude ψ^{ref} can be set as (42) to achieve field weakening operation.

$$\psi_1^{ref} = \min(\psi^{ref}, \frac{U_{dc}}{\sqrt{3}\omega_e}) \tag{42}$$

B. Starting method Based on Sensorless MPFC

To achieve sensorless operation of MPFC, the AFO described in previous section is incorporated and the estimated speed $\hat{\omega}_r$ instead of ω_r is used in (1) to calculate the prediction of concerned variables.

During the estimation of free-running speed, the torque reference is set as zero and the reference of stator flux is given in a feed-forward fashion as

$$\boldsymbol{\psi}_s^{ref} = \psi^{ref} e^{j\theta^{ref}} \tag{43}$$

$$\theta^{ref} = \int_0^T \hat{\omega}_r dt \tag{44}$$

The initial value of $\hat{\omega}_r$ is set as zero, so that estimated speed can respond to both rotational direction quickly. To avoid triggering over-current protection, the limitation of current amplitude is added in the cost function as

$$J_1 = |\boldsymbol{\psi}_s^{ref} - \boldsymbol{\psi}_s^{k+2}| + I_{oc} \tag{45}$$

$$I_{oc} = \begin{cases} 10^3 + 10^3(|\boldsymbol{i}_s^{k+2}| - I_{max}) & \text{if } |\boldsymbol{i}_s^{k+2}| > I_{max} \\ 0 & \text{if } |\boldsymbol{i}_s^{k+2}| < I_{max} \end{cases} \tag{46}$$

where $\boldsymbol{i}_s^{k+2}$ can be predicted using first row of (1) based on $\boldsymbol{i}_s^{k+1}$ in the first-step prediction. I_{max} is the allowed amplitude of stator current. (46) is used to generate a large value of cost function when a given voltage vector leads to excess of current limitation. Therefore, this voltage vector will be excluded because the optimal voltage vector is determined based on minimization of cost function. As the weighting factor for current limitation set as 1000 in (46) is much larger than the amplitude of stator flux vector, the voltage vector resulting in over-current would not be selected. In this way, the stator current can be effectively kept below the limitation during dynamic process.

Unlike current limitation introduced in [25], not only a fixed value is added to the cost function, but also the excess of current limitation is considered when $|\boldsymbol{i}_s^{k+2}| > I_{max}$. Hence, if all the predicted $|\boldsymbol{i}_s^{k+2}|$ exceeds I_{max}, the voltage vector which results in the current variation pointing to minimal amplitude will be selected, increasing the robustness against noise and inaccurate speed information. As the prediction of current during each control period is based on the measured value, there would be no accumulating error. Additionally, the sampling frequency adopted in this paper is as high as 20 kHz, prediction errors would be small enough and stator current can be well controlled with no obvious excess of the limitation during starting process. Nevertheless, if higher accuracy of prediction is required, the closed loop predictor may be used as shown in [1]. The remaining question is to judge when the estimation of rotating speed should be terminated and shift to normal operation.

From (1)-(4), the following equation can be obtained.

$$p\boldsymbol{\psi}_r = \lambda L_m R_r \boldsymbol{\psi}_s - (\lambda L_s R_r - j\omega_r)\boldsymbol{\psi}_r \tag{47}$$

As the output frequency of the inverter is $\hat{\omega}_r$ during estimation of free-running speed, the following equation can be obtained based on (47).

$$\boldsymbol{\psi}_r = \frac{\lambda L_m R_r \boldsymbol{\psi}_s}{j(\hat{\omega}_r - \omega_r) + \lambda L_s R_r} \tag{48}$$

It can be seen that if there is a large difference between $\hat{\omega}_r$ and ω_r, the amplitude of $\boldsymbol{\psi}_r$ would be much less than that of $\boldsymbol{\psi}_s$. And if there is no error between between $\hat{\omega}_r$ and ω_r, the amplitude of $\boldsymbol{\psi}_r$ would be

$$|\boldsymbol{\psi}_r| = \frac{L_m}{L_s} |\boldsymbol{\psi}_s| \tag{49}$$

Hence, smaller error between $|\boldsymbol{\psi}_r|$ and $L_m |\boldsymbol{\psi}_s| / L_r$ represents smaller error between $\hat{\omega}_r$ and ω_r. In practical applications, when (50) is satisfied, the starting process is terminated and normal operation is subsequently enabled.

$$\left|\hat{\boldsymbol{\psi}}_r\right| > \frac{f \cdot L_m}{L_s}\psi^{ref} \tag{50}$$

where f is a parameter and $f < 1$. In (50), the reference of stator flux magnitude ψ^{ref} is used instead of $|\boldsymbol{\psi}_s|$ for better robustness and reliability. $\hat{\boldsymbol{\psi}}_r$ is calculated from (4), in which the current is directly measured. Thus the accuracy of $\hat{\boldsymbol{\psi}}_r$ depends on $\hat{\boldsymbol{\psi}}_s$. As can be seen from (6) and the second row of matrix A in (1), there is no speed involved in the estimation of stator flux but only the error of current estimation is involved. Hence the accuracy of $\hat{\boldsymbol{\psi}}_s$ would be affected by current error. Since the current estimation is a closed-loop system in AFO, the current estimation error would be small enough and has little impact on the estimation of stator flux. Namely, it can be assumed that $\hat{\boldsymbol{\psi}}_s$ has good accuracy. In brief, (50) is accurate enough to judge whether $\hat{\omega}_r$ is close to ω_r. As can be seen from (48), the amplitude of rotor flux would be very small if there is a large error between estimated speed and actual speed. Hence, the rotor flux can only be build up when the speed estimation error is small enough. In this paper, f is selected as 0.8 based on the consideration that the rotor flux has been close to rated value and speed estimation error is small enough in this condition. Consequently, the control system could be safely shifted to normal operation. The overall flow chart of the proposed method is shown in Fig. 3. The variable $flag$ in the figure represents different operating mode, which is initialized as 0. $flag = 0$ means the control system is estimating free-running speed while $flag = 1$ means the normal operation is enabled.

It should be noted that after the estimation of free-running speed, the feedback gain matrix can be switched to other types optimized for normal operation, such as those listed in [1], [14], [26]. In this paper, the gain matrix shown in (51) will be used during normal operation [26].

$$\boldsymbol{G} = -\begin{bmatrix} 2b \\ b/(\lambda L_r) \end{bmatrix} \tag{51}$$

where b is a constant negative gain.

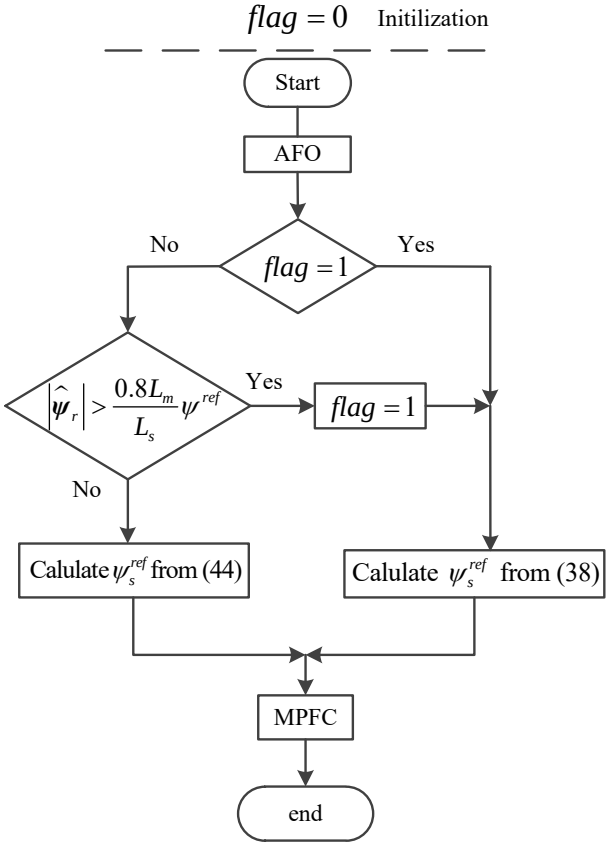

Fig. 3. Flow chart of the proposed method

TABLE I
PARAMETERS OF IM AND CONTROL SYSTEM

Rated power	P_N	2.2 kW
DC-bus voltage	U_{dc}	540 V
Rated voltage	U_N	380 V
Rated frequency	f_N	50 Hz
Number of pole pairs	N_p	2
Stator resistance	R_s	1.76 Ω
Rotor resistance	R_r	1.29 Ω
Mutual inductance	L_m	0.158 H
Stator inductance	L_s	0.170 H
Rotor inductance	L_r	0.170 H
Maximum stator current	I_{max}	10 A
Control Period	T_{sc}	50 μs
Flux magnitude	ψ^{ref}	0.8 Wb

V. Simulation and Experimental Tests

A. Simulation Results

To validate the effectiveness of the proposed method, it is tested in the Matlab/Simulink with a two level inverter fed IM drive. Parameters of machine and control system are shown in table I. As speed estimator in AFO is a multi-variable, complex nonlinear system, it is hard to evaluate the influence of parameter h in gain matrix (37) on the free-running speed estimation by theory analysis. Hence, it is studied in simulation and the results with different h are shown in Fig. 4. It is seen that larger h leads to slower dynamic responses. During the estimation of free-running speed, the estimation of current error mainly results from incorrect speed. A larger h introduces stronger feedback of current error to correct estimated current $\hat{\boldsymbol{i}}_s$. Hence, the effect caused by incorrect speed is decreased, resulting in longer settling time. According to Fig. 4, h is set as -0.5 in the following tests. For optimal selection of h, further research still needs to done in an analytical way. It should be noted that a negative h can amplify the current error caused by incorrect speed, which can speed up the identification of free-running speed. The same feature can also be seen in the feedback gain design to improve the stability and robustness during low speed regenerating operation [18].

In the following tests, the last curve of variable $flag$ in each figure represents operating mode. The value of $flag$ changes from 0 to 1 means the estimation of free-running speed is terminated and the normal operation is enabled. Before the control system is activated, the motor is initially free-running at 1500 rpm and the speed reference is set as 2100 rpm. The I_{max} in (46) is set as 10 A.

Fig. 5 shows the simulated responses of starting a rotating

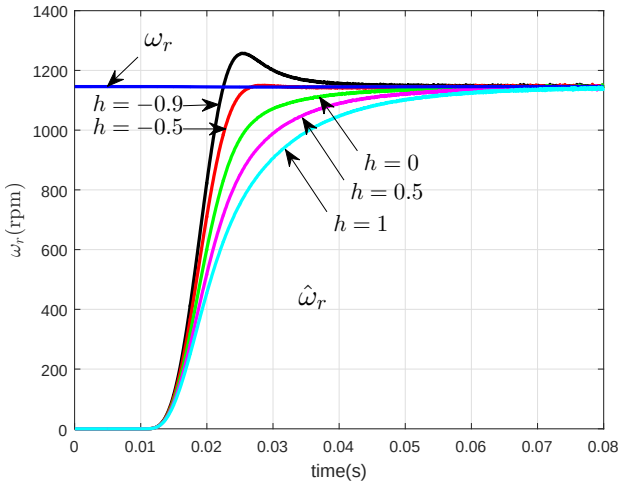

Fig. 4. Simulated responses with different values of h in (37)

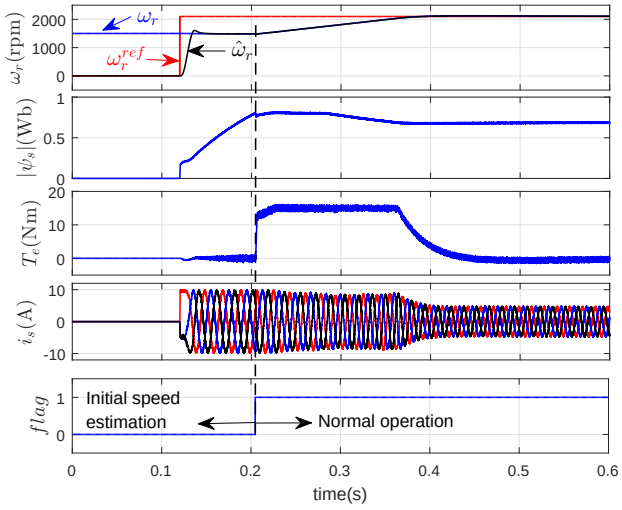

Fig. 5. Simulated starting responses with proposed method

motor with the proposed method. It takes less than 0.1s for estimating initial speed. Stator currents are sinusoidal without excess of limitation during the whole process. After shifting to normal operation, the closed-loop control is enabled and the motor is accelerated quickly to the reference. Above base speed, the magnitude of stator flux is decreased to achieve field-weakening operation. During dynamic process, the estimated speed accurately follows actual speed and the torque is well controlled without oscillation. This test validates that smooth and quick start of a motor rotating at high speed can be achieved based on the proposed method.

For achieving better steady state performance, the proposed starting scheme can also be implemented with MPFC using two optimal voltage vectors [27]. The simulated results can be seen in Fig. 6. It can be seen that the estimated speed quickly approaches to actual speed. The whole response is very similar to that in Fig. 5. However, it is obvious that torque ripple in Fig. 6 is significantly lower because more voltage vectors are applied in one control period.

To illustrate the effectiveness of the proposed feedback gain

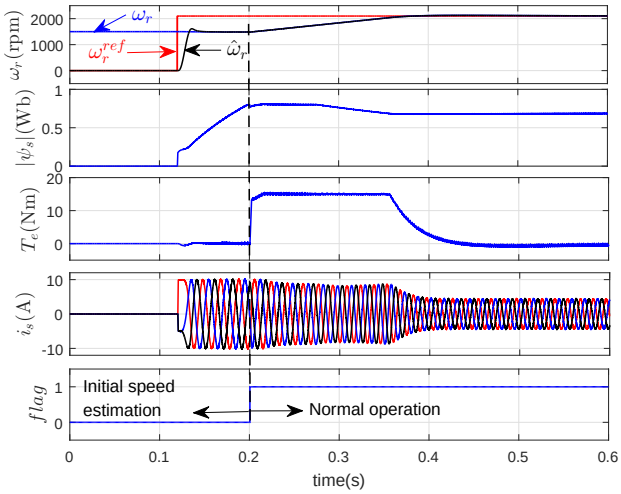

Fig. 6. Simulated starting responses with the proposed scheme based on MPFC in [27]

matrix, the responses under the same conditions are recorded in Fig. 7 for zero gain matrix and (51). It can be seen that $\hat{\omega}_r$ can not converge to ω_r in both cases. However, the stator current is still well controlled without obvious excess of limitation. This indicates that current amplitude can be effectively limited by (45) and (46) even with incorrect speed information.

To validate the effectiveness of deduced condition (30), the initial value of $\hat{\omega}_r$ is set as 2500 rpm. It is shown in Fig. 8 that the estimated speed can converge to actual speed quickly. Similar to that in Fig. 5, the motor is accelerated to the speed reference after the estimation of free-running speed. This test shows that a smooth and fast start of a rotating motor can be achieved by setting the initial estimated speed as the maximum operating speed. However, the main drawback of this solution is that the rotational direction must be known in advance to determine whether positive or negative maximum speed is set as initial value of $\hat{\omega}_r$. As can be seen from Fig. 9, if the rotational direction is wrongly identified at the beginning, the estimated speed can not converge to actual speed and starting of the rotating motor fails. Hence, the proposed method with gain matrix (37) is more universal and simpler for implementation.

B. Experimental Results

The proposed method is experimentally verified on a two-level inverter-fed IM drive platform. The developed algorithm is implemented on a 32bit floating point DSP TMS320F28335. The internal variables are displayed on digital oscilloscope via on-board DA converter. The waveform of stator current is directly obtained by a current probe. During the following tests, the actual speed is measured through an incremental encoder, which is not used in the control algorithm but only displayed on oscilloscope for comparison. The machine and control parameters are the same as those used in simulation tests. Curves of four channels recorded by the oscilloscope are actual speed, estimated speed, magnitude of estimated stator flux and stator current respectively. For a direct comparison

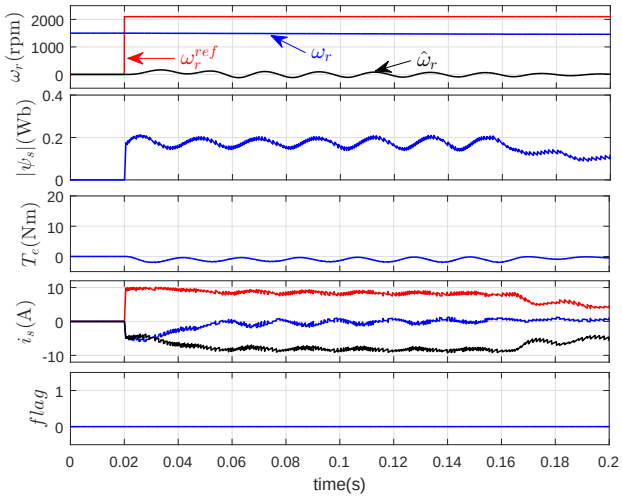

(a)

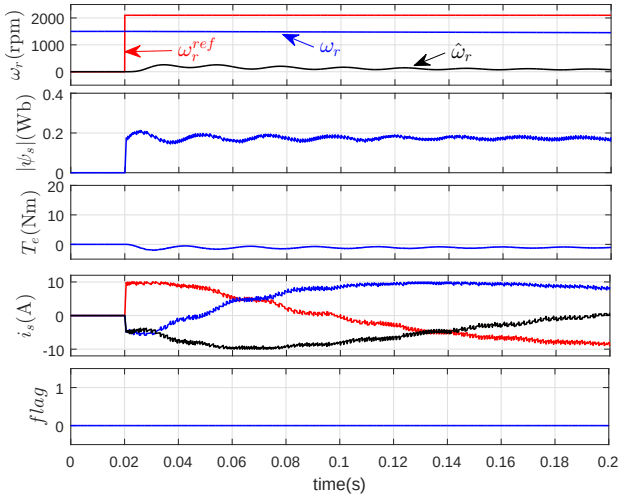

(b)

Fig. 7. Simulated starting process with (a) zero gain matrix and (b) gain matrix (51)

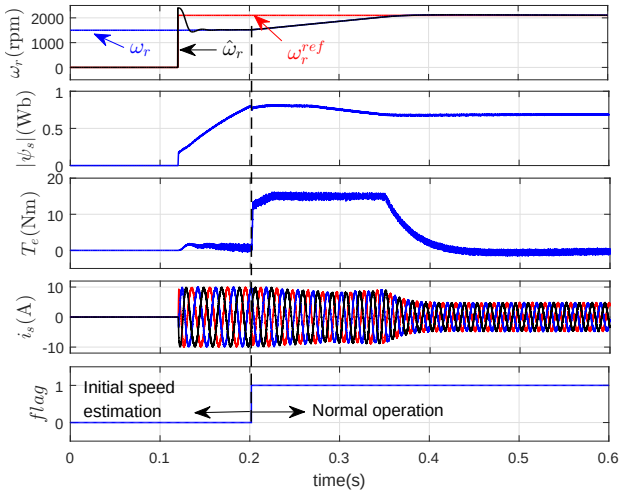

Fig. 8. Simulated starting responses with zero gain matrix and the initial value of $\hat{\omega}_r$ is set as maximum operating speed

of actual speed and estimated speed, their zero positions are

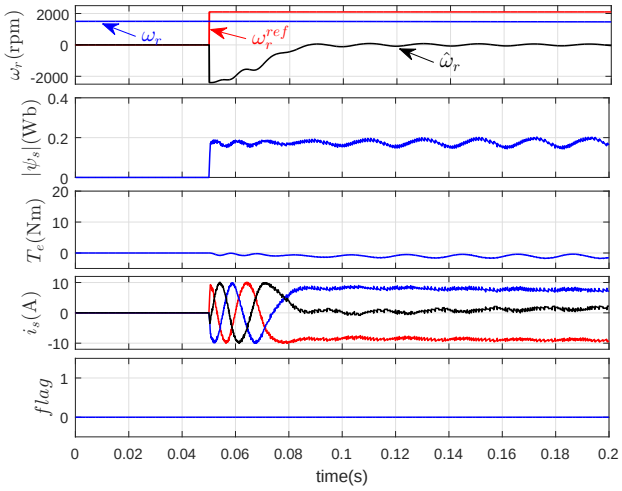

Fig. 9. Simulated starting responses with zero gain matrix and the initial value of $\hat{\omega}_r$ is set as opposite direction

set the same.

Fig. 10 shows responses when the machine restarts from forward speed. At the beginning, the motor is rotating at 2250 rpm. Then, the power is turned off and control system is reset. When the power is off, rotor speed decreases gradually due to friction load. After a short time, the control system is reactivated and the motor is re-accelerated to 2250 rpm. It can be found that, the estimated speed can converge to actual speed quickly with the proposed method. There is no large inrush current and stator current is well controlled with no obvious excess of the limitation (10A) during the restarting process. Above the base speed, flux magnitude is decreased to achieve field-weakening operation. The same test is investigated when the motor restarts from backward speed. The motor is initially rotating at -2250 rpm. The inverter is turned off and then turned on. After the estimation of free-running speed, the motor is re-accelerated to -2250 rpm. The results are shown in Fig. 11. The responses are similar to that in Fig. 10. In Fig. 12, the curve of estimated electromagnetic torque is included when starting from forward speed. Due to fast estimation of free-running speed, inverter output frequency is quickly synchronized with the rotating speed of the motor. It can be seen that torque is stably controlled without oscillation during starting process and it quickly increases to maximum value after the estimation of free-running speed. From these tests, it is clear that the proposed method can effectively start a rotating motor from both rotational direction smoothly and quickly.

Fig. 13 shows responses of starting process when the feedback gain matrix is set as zero. It is clear that, without properly designed feedback gain matrix, the estimated speed can not converge to real speed when there is a large difference between two variables. This test confirms that a proper design of feedback gain matrix is essential for fast starting of a rotating motor when the initial speed is set as zero. As the actual speed decreases due to friction load, the difference between ω_r and $\hat{\omega_r}$ becomes smaller and smaller. It can be seen that if $\triangle\omega_r$ becomes small enough, the stable and fast control of motor can still be achieved. However, it would be

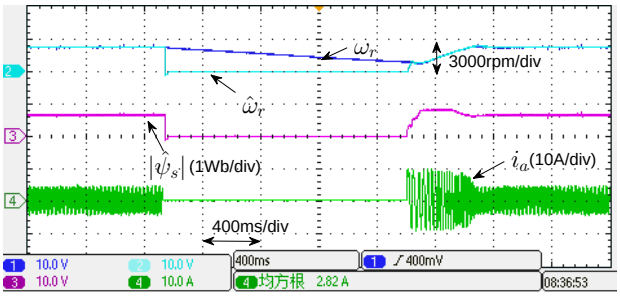

Fig. 10. Restarting from forward speed with the proposed method

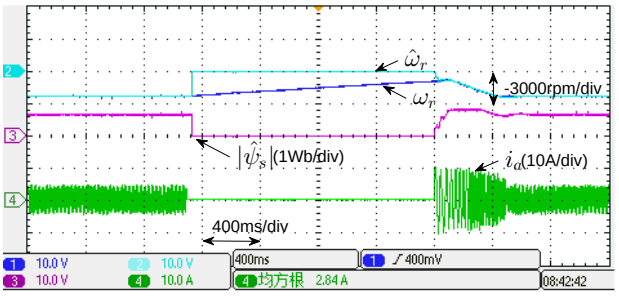

Fig. 11. Restarting from backward speed with the proposed method

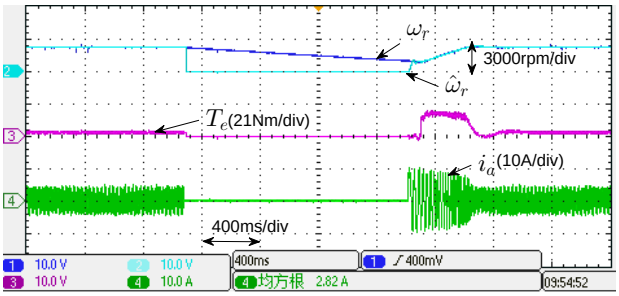

Fig. 12. Actual speed, estimated speed, torque, and stator current waveforms during restarting process with the proposed method

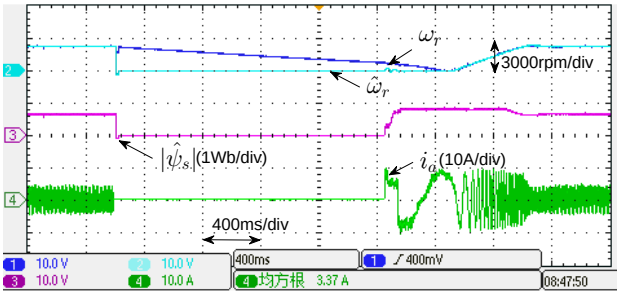

Fig. 13. Restarting with zero feedback gain matrix

time consuming to wait for speed to decrease with a large shaft inertial. And it is not suitable for starting a machine rotated by external load, because the motor would not stop in this substation unless the external load is disconnected. For example, in the application of fan and turbine, the motor may be rotated by water and wind flow.

As analyzed in section III-B, if initial estimated speed is set as the maximum operating speed with the same sign of the actual speed, the rotating motor can be started when the feedback gain matrix is set as zero. The response is shown in Fig.14. Compared with the results in Fig. 13, the free-running motor is re-accelerated quickly to the reference after the control system is reactivated, not having to wait for the motor speed to decrease to zero. As shown in simulation results, the main problem of this method is that the rotational direction must be known or accurately estimated before setting the initial value of $\hat{\omega}_r$, increasing the complexity of implementation.

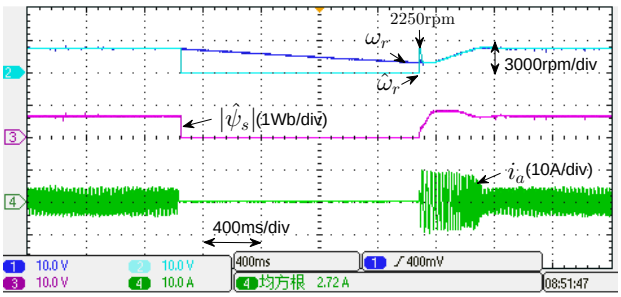

Fig. 14. Restarting with zero feedback gain matrix and the initial value of $\hat{\omega}_r$ is set as 2250 rpm

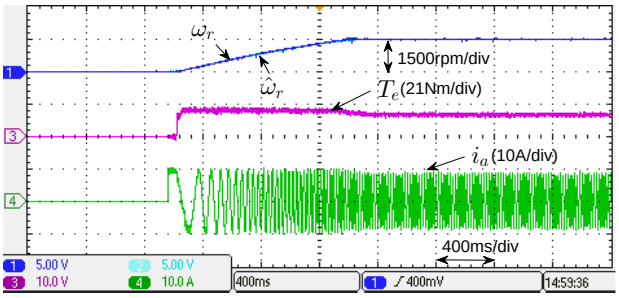

Fig. 15. Starting from standstill with rated load based on the proposed method

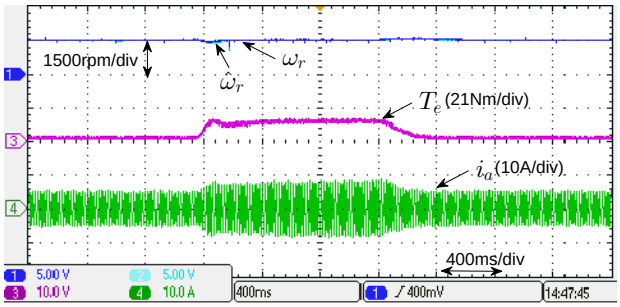

Fig. 16. Tested results during load change at 1500 rpm

Fig. 15 shows the responses when starting from standstill to 1500 rpm based on the proposed method. Before starting the machine, 14 Nm resistance load (full load) is applied by a magnetic powder brake. It can be seen that the proposed speed-sensorless scheme can achieve smooth start with 100% rated load. The waveforms of $\hat{\omega}_r$ and ω_r almost coincides with each other, validating that the estimated speed has good accuracy over a wide speed range. During the whole process, there is no oscillation and the system is well controlled without inrush of current.

The robustness of the control system against external load

disturbance is also tested. The results are presented in Fig. 16. During the whole process, the speed reference is kept at 1500 rpm. At the beginning, the motor is steadily running at 1500 rpm without load. After a moment, an external load is suddenly applied for a short time. It can be seen that there is a slight drop of rotor speed when the load is applied, but the speed returns to its reference quickly, showing good robustness against external load disturbance.

VI. Conclusion

This paper proposes a method for starting a free running IM without speed sensor. The convergence condition of speed estimation for AFO is analyzed during restarting process. Then a feedback gain matrix is deduced to eliminate the necessity of estimation of rotational direction while guaranteeing the estimated speed can converge to any initial speed. The integration of proposed AFO into FCS-MPFC is illustrated. The reference generation and current limitation during starting process are designed to achieve safe, smooth and quick restarting. The effectiveness of the proposed method is verified by both simulation and experimental tests.

For application to high power drives, the penalty of switching effort should be included in the cost function for limiting switching frequency. Additionally, multi-step prediction may be required in order to obtain better steady state performance.

References

[1] S. A. Davari, D. A. Khaburi, F. Wang, and R. M. Kennel, "Using full order and reduced order observers for robust sensorless predictive torque control of induction motors," *IEEE Trans. Power Electron.*, vol. 27, no. 7, pp. 3424–3433, July 2012.

[2] T. Geyer, "Computationally efficient model predictive direct torque control," *IEEE Trans. Power Electron.*, vol. 26, no. 10, pp. 2804 –2816, oct. 2011.

[3] M. Habibullah and D. D. C. Lu, "A speed-sensorless fs-ptc of induction motors using extended kalman filters," *IEEE Trans. Ind. Electron.*, vol. 62, no. 11, pp. 6765–6778, Nov 2015.

[4] T. Geyer and D. Quevedo, "Multistep finite control set model predictive control for power electronics," *IEEE Trans. Power Electron.*, vol. 29, no. 12, pp. 6836–6846, Dec 2014.

[5] Y. Zhang and H. Yang, "Model-predictive flux control of induction motor drives with switching instant optimization," *IEEE Trans. Energy Convers.*, vol. 30, no. 3, pp. 1113–1122, Sept 2015.

[6] J. Rodriguez, R. Kennel, J. Espinoza, M. Trincado, C. Silva, and C. Rojas, "High-performance control strategies for electrical drives: An experimental assessment," *IEEE Trans. Ind. Electron.*, vol. 59, no. 2, pp. 812 –820, feb. 2012.

[7] Y. Zhang, B. Xia, and H. Yang, "Performance evaluation of an improved model predictive control with field oriented control as a benchmark," *IET Electr. Power Appl.*, 2016, in press.

[8] C. Rojas, J. Rodriguez, F. Villarroel, J. Espinoza, C. Silva, and M. Trincado, "Predictive torque and flux control without weighting factors," *IEEE Trans. Ind. Electron.*, vol. 60, no. 2, pp. 681 –690, feb. 2013.

[9] F. Wang, Z. Chen, P. Stolze, J. F. Stumper, J. Rodriguez, and R. Kennel, "Encoderless finite-state predictive torque control for induction machine with a compensated mras," *IEEE Trans. Ind. Informat.*, vol. 10, no. 2, pp. 1097–1106, May 2014.

[10] Y. Zhang and H. Yang, "Model predictive torque control of induction motor drives with optimal duty cycle control," *IEEE Trans. Power Electron.*, vol. 29, no. 12, pp. 6593–6603, 2014.

[11] P. Karamanakos, P. Stolze, R. Kennel, S. Manias, and H. du Toit Mouton, "Variable switching point predictive torque control of induction machines," *IEEE Trans. Emerg. Sel. Topics Power Electron.*, vol. 2, no. 2, pp. 285–295, 2014.

[12] D. Marcetic, I. Krcmar, M. Gecic, and P. Matic, "Discrete rotor flux and speed estimators for high-speed shaft-sensorless im drives," *IEEE Trans. Ind. Electron.*, vol. 61, no. 6, pp. 3099–3108, June 2014.

[13] I. M. Alsofyani and N. R. N. Idris, "Simple flux regulation for improving state estimation at very low and zero speed of a speed sensorless direct torque control of an induction motor," *IEEE Trans. Power Electron.*, vol. 31, no. 4, pp. 3027–3035, April 2016.

[14] W. Sun, Y. Yu, G. Wang, B. Li, and D. Xu, "Design method of adaptive full order observer with or without estimated flux error in speed estimation algorithm," *IEEE Trans. Power Electron.*, vol. 31, no. 3, pp. 2609–2626, March 2016.

[15] K. Fujinami, K. Takahashi, K. Kondo, and Y. Sato, "A restarting method of an induction motor speed-sensorless vector control system for a small-sized wind turbine power generator system," in *Int. Conf. on Elect. Mach. and Syst.*, Nov 2009, pp. 1–5.

[16] K. Kondo, "Pmsm and im rotational sensorless technologies specialized for railway vehicles traction," in *IEEE 5th Int. Symp. on Sensorless Control for Elect. Drives*, May 2014, pp. 1–7.

[17] L. Harnefors and M. Hinkkanen, "Stabilization methods for sensorless induction motor drives–a survey," *IEEE Trans. Emerg. Sel. Topics Power Electron.*, vol. 2, no. 2, pp. 132–142, June 2014.

[18] W. Sun, J. Gao, Y. Yu, G. Wang, and D. Xu, "Robustness improvement of speed estimation in speed-sensorless induction motor drives," *IEEE Trans. Ind. Appl.*, vol. 52, no. 3, pp. 2525–2536, May 2016.

[19] M. Zaky, "Stability analysis of speed and stator resistance estimators for sensorless induction motor drives," *IEEE Trans. Ind. Electron.*, vol. 59, no. 2, pp. 858 –870, feb. 2012.

[20] L. Harnefors and M. Hinkkanen, "Complete stability of reduced-order and full-order observers for sensorless im drives," *IEEE Trans. Ind. Electron.*, vol. 55, no. 3, pp. 1319–1329, March 2008.

[21] H. Iura, K. Ide, T. Hanamoto, and Z. Chen, "An estimation method of rotational direction and speed for free-running ac machines without speed and voltage sensor," *IEEE Trans. Ind. Appl.*, vol. 47, no. 1, pp. 153–160, Jan 2011.

[22] S. J. Jeong, Y. M. Park, and G. J. Han, "An estimation method of rotation speed for minimizing speed variation on restarting of induction motor," in *IEEE 8th Int. Conf. on Power Electron. and ECCE Asia*, May 2011, pp. 697–704.

[23] J. Maes and J. Melkebeek, "Speed-sensorless direct torque control of induction motors using an adaptive flux observer," *IEEE Trans. Ind. Appl.*, vol. 36, no. 3, pp. 778–785, 2000.

[24] H. Kubota, K. Matsuse, and T. Nakano, "Dsp-based speed adaptive flux observer of induction motor," *IEEE Trans. Ind. Appl.*, vol. 29, no. 2, pp. 344–348, Mar 1993.

[25] H. Miranda, P. Cortes, J. Yuz, and J. Rodriguez, "Predictive torque control of induction machines based on state-space models," *IEEE Trans. Ind. Electron.*, vol. 56, no. 6, pp. 1916 –1924, june 2009.

[26] Y. Zhang, J. Zhu, Z. Zhao, W. Xu, and D. Dorrell, "An improved direct torque control for three-level inverter-fed induction motor sensorless drive," *IEEE Trans. Power Electron.*, vol. 27, no. 3, pp. 1502 –1513, march 2012.

[27] Y. Zhang and H. Yang, "Two-vector-based model predictive torque control without weighting factors for induction motor drives," *IEEE Trans. Power Electron.*, vol. 31, no. 2, pp. 1381–1390, Feb 2016.